

Intrinsic magnetism at silicon surfaces*

Steven C. Erwin¹ and F. J. Himpsel²

¹*Center for Computational Materials Science, Naval Research Laboratory, Washington, DC 20375, USA*

²*Department of Physics, University of Wisconsin-Madison, Madison, WI 53706, USA*

(Dated: April 23, 2010 (submitted version))

It has been a long-standing goal to create magnetism in a nonmagnetic material by manipulating its structure at the nanometer scale. This idea may be realized in graphitic carbon: evidence suggests magnetic states at the edges of graphene ribbons and at grain boundaries in graphite. Such phenomena have long been regarded as unlikely in silicon because there is no graphitic bulk phase. Here we show theoretically that intrinsic magnetism indeed exists in a class of silicon surfaces whose step edges have a nanoscale graphitic structure. This magnetism is intimately connected to recent observations, including the coexistence of double- and triple-period distortions and the absence of edge states in photoemission. Magnetism in silicon may ultimately provide a path toward spin-based logic and storage at the atomic level.

Individual atoms with an odd number of electrons exhibit a magnetic moment from the spin of the unpaired electron. Elements with an even number of electrons, such as carbon and silicon, can also reveal unpaired electrons when covalent bonds are broken. In defective or disordered group-IV solids the single electrons that occupy dangling bonds can be detected in magnetic resonance experiments, but the lack of long-range structural order precludes a magnetically ordered state.

Bonds are also broken at the surfaces and interfaces of solids, but covalent materials usually reconstruct to eliminate dangling bonds or doubly occupy them with electrons of opposite spin. Exceptions to this behavior provide fertile ground for magnetism in nonmagnetic materials. Two widely discussed examples are based on graphitic carbon: highly oriented pyrolytic graphite exhibits ferromagnetic order arising from two-dimensional arrays of defect spins at grain boundaries,¹ and nanoscale graphene ribbons are predicted to have ferromagnetically ordered edge states.²

The edges of graphene ribbons are theoretically appealing but far from being realized experimentally with the required atomic smoothness. Other one-dimensional systems such as nanowires³ and step edges provide more favorable conditions for long-range structural order and thus are promising platforms for devices requiring ordered arrays of spins. Indeed, atomically smooth steps with structural order extending to micrometers can be produced by self-assembly at vicinal silicon surfaces. Some of these surfaces naturally form a graphitic silicon ribbon at the step edge. Here we predict, using density-functional theory (DFT, see Methods), that the electronic ground state of these silicon surfaces is magnetic. Magnetism in silicon systems having no magnetic elements is quite unexpected. Indeed, none of these systems has yet been investigated for magnetism experimentally, but we show below that existing data already support it indirectly.

Our discussion focuses on the Si(553)-Au and Si(557)-Au surfaces, shown in Fig. 1. These are stepped surfaces stabilized by a fraction of a monolayer of Au. Crystallographically they can be considered miscut from the flat

Si(111) surface by angles of 12.3° and 9.4° away from and toward, respectively, the (001) orientation. They are members of a family of Au-induced vicinal silicon surfaces intermediate between (111) and (001) containing several structural motifs in common.⁴ These commonalities suggest that magnetism in silicon may be widespread.

The critical structural motif for magnetism in these systems is a nanoscale honeycomb strip of graphitic silicon, just a single hexagon wide, that forms the edge of the step.⁵ This honeycomb chain was first observed in reconstructions of flat Si(111) induced by submonolayer coverages of alkali, alkaline-earth, and some rare-earth metals, as well as Ag and Au.⁶ In these flat surfaces the orbitals of the outer honeycomb atoms form filled bands, either by accepting electrons from the adsorbates or by forming partially covalent bonds. At a step edge a new possibility arises in which these orbitals are singly occupied, fully spin polarized, and magnetically ordered.

The two surfaces studied here have step edges with opposite orientation. The DFT ground state (see Methods) depicted in Fig. 1a for Si(553)-Au shows every third Si atom at the step edge to be completely spin polarized while all other atoms are negligibly polarized. On Si(557)-Au (Fig. 1c) every second Si atom at the step is fully polarized as are all the terrace restatoms. In both systems the interaction between neighboring spins along a step is antiferromagnetic.

These predictions depend on an accurate knowledge of the atomic structure of each surface. The model of Si(557)-Au shown in Fig. 1c is well-established from DFT calculations^{4,7} and X-ray diffraction.⁸ The energy bands measured in Si(557)-Au agree well with the calculated bands arising from the Au chains. A small band splitting^{9–12} originates from the spin-orbit interaction of the Au atoms.^{7,13} In this “Rashba effect”—which is unrelated to the magnetism we predict here—the two split bands have a spin polarization of 100% at any given momentum in reciprocal space, but this vanishes when integrated over all momenta and leaves no net spin polarization in real space.

Existing models for the structure of the Si(553)-Au surface do not reproduce the experimental band

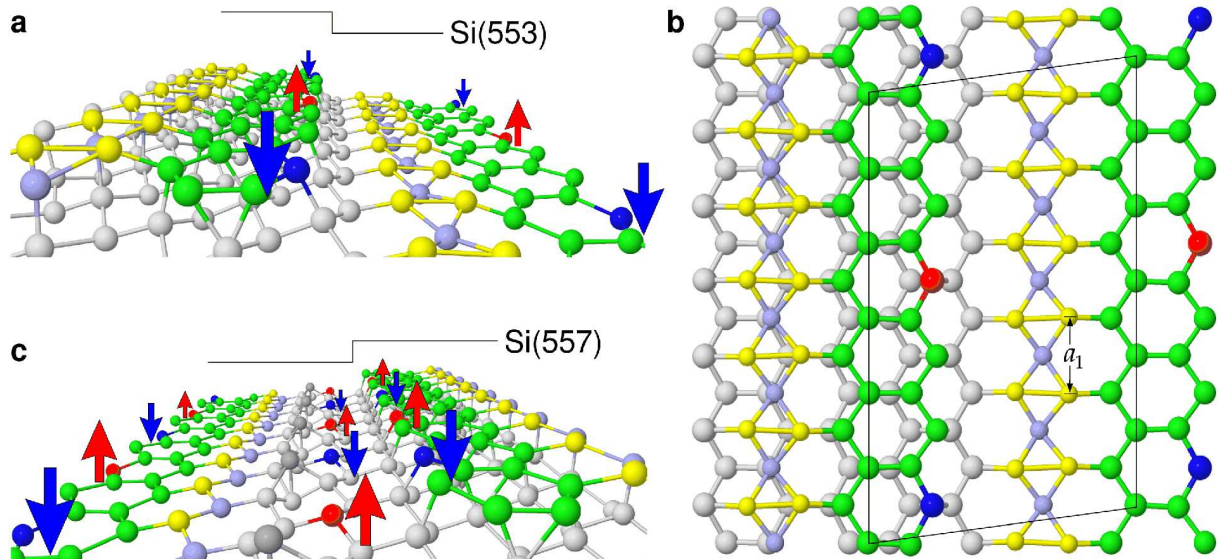


FIG. 1: **Ground state structure and lowest energy spin configuration of two magnetic silicon surfaces.** a–b, Si(553)-Au in its antiferromagnetic ground state. Yellow atoms are Au, all others are Si. Each terrace contains a Au double row and a graphitic Si honeycomb chain (green) at the step edge. Every third Si (red, blue) at the step has a spin magnetic moment of one Bohr magneton ($S = 1/2$, arrows) from the complete polarization of the electron occupying the dangling-bond orbital. The sign of the polarization alternates along the step. The periodicity along the step is tripled by a small downward displacement of the magnetic atoms. The periodicity along the two Au rows is doubled, with alternating short and long bonds a_1 . The full 1×6 unit cell is outlined. c, Si(557)-Au in its antiferromagnetic ground state. The step direction of Si(557) is opposite to that of Si(553) as shown by the schematic outlines. Nevertheless this surface is also magnetic: every second Si (red, blue) at the step has a magnetic moment of one Bohr magneton, as do all of the Si restatoms (blue, red) on the terrace.

structure.^{14,15} We demonstrate below that the model proposed in Fig. 1a correctly predicts not only the band structure, but also the previously unexplained coexistence of two periodicities observed in scanning tunneling microscopy (STM). We also show that these predictions are inextricably linked with magnetic order. Their experimental confirmation constitutes indirect but compelling evidence for the existence of magnetism as well.

The Si(553)-Au surface was first observed in Ref. 16 and its unusual one-dimensional electronic properties have since been extensively studied. Two experimental findings are especially striking. (1) STM images acquired at room temperature show alternating bright and dim rows, each with the periodicity of the Si surface lattice constant a_0 .^{17–20} At temperatures below 50 K these rows separately develop higher-order periodicity: a tripled period ($3a_0$) for the bright rows and a doubled period ($2a_0$) for the dim rows. These effects have variously been attributed to periodic lattice distortions¹⁸ and to charge-density waves,¹⁹ but their true microscopic origin has remained elusive. (2) Angle-resolved photoemission spectra (ARPES) obtained at 160–220 K reveal three metallic bands, all with their minima at the zone boundary ZB_{\parallel} of the 1×1 Brillouin zone.¹⁶ The two lower bands are slightly split by a small momentum splitting $\delta k_F = 0.05 \text{ \AA}^{-1}$,¹³ and cross the Fermi level about halfway to the zone center. Detailed analysis of this crossing shows that the splitting is due to the spin-orbit

interaction.¹³ The upper band crosses the Fermi level about one-fourth of the way to the zone center without a detectable splitting.

All of these observations are correctly predicted by the proposed model of Si(553)-Au. Figure 2 shows the theoretical simulated STM image for the model in Fig. 1a in its antiferromagnetic ground state. The bright row arises from Si atoms at the step edge and indeed has tripled periodicity $3a_0$. The highest peaks within this row are from the spin-polarized atoms. This appears counterintuitive since these atoms are actually 0.3 \AA below the height of their non-polarized neighbors. Moreover, the dangling-bond orbital on this atom is occupied by a single electron rather than two. But the average energy of the occupied spin-polarized orbital is energetically closer to the Fermi level and as a result the topography appears higher in filled-state tunneling.

The dim second row visible in Fig. 2a arises from the right-hand leg of the ladder formed by two rows of Au atoms. Its doubled periodicity $2a_0$ is due to the dimerization created when the rungs of this ladder rotate with alternating signs along a row. A similar dimerization occurs in a closely related system, Si(111)- (5×2) -Au, where it is driven by electron doping from Si adatoms and the consequent formation of a surface band gap.²¹ For Si(111)- (5×2) -Au the dimerization parameter $d = (a_1 - a_0)/a_0$, where a_0 is the surface lattice constant and a_1 is defined in Fig. 1b, has the value $d = 0.14$, much

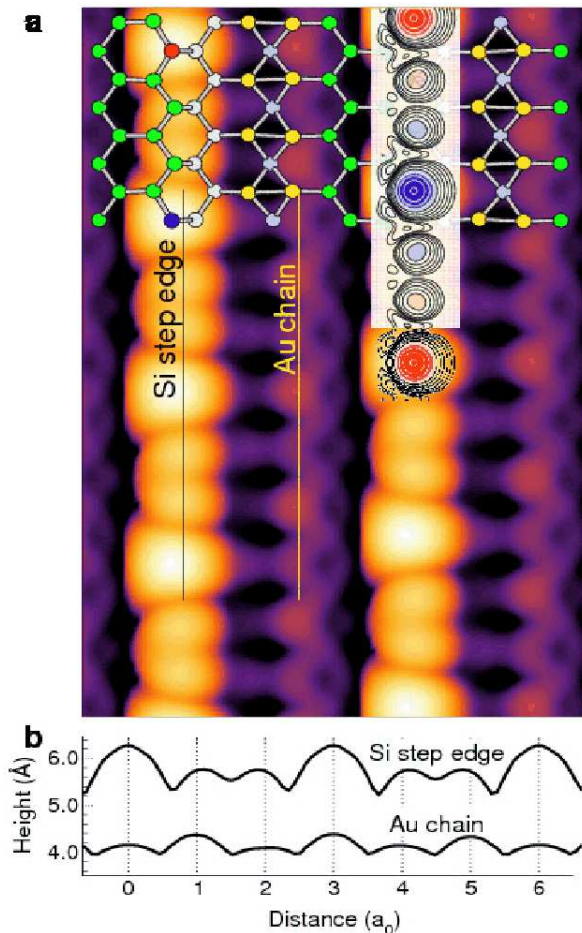


FIG. 2: **Scanning tunneling microscopy of Si(553)-Au.** **a**, Theoretical STM topography showing the tip height at constant current for tunneling into empty surface states at bias voltage +0.5 V. Inset: Electron spin density 1 Å above the step edge. Red and blue contours represent positive and negative polarization, indicating antiferromagnetic alignment of the red and blue Si atoms the step edge. Contours are separated by a factor of two. **b**, Line scans at the locations marked in **a**, showing the coexisting $3a_0$ and $2a_0$ periodicity along the Si step edge and Au chain, respectively.

larger than the value $d = 0.04$ for Si(553)-Au. But even this small dimerization is sufficient to produce a doubled periodicity that is well-resolved in the theoretical STM image.

The spin polarization of the electron density, shown in the inset to Fig. 2a, is strongly localized at every third Si step-edge atom. Integrating this spin density shows that the red and blue step-edge atoms each have a spin moment of 1 Bohr magneton, equivalent to a fully polarized electron with spin $S = 1/2$. The direction of the spin alternates along the step in this antiferromagnetic ground state. Moments on other atoms along the step are smaller by an order of magnitude.

The connection between magnetism and the periodicity of the rows is simple and direct. If the spin polariza-

tion is constrained to be zero then the DFT equilibrium geometry of the model changes: both the tripled periodicity along the Si rows and the doubled periodicity along the Au rows are completely eliminated. In this sense the experimental observation of triple and double periodicities constitutes strong evidence for a spin-polarized ground state.

Magnetism also provides the key to understanding a long-standing puzzle presented by ARPES data for Si(553)-Au. The orbitals at the step edges of a vicinal surface would normally give rise to sharp electronic states near the Fermi level, as is indeed the case for previously proposed models of Si(553)-Au.^{14,15} But these are not observed in the ARPES data. We demonstrate below that spin polarization at the step edge provides the resolution to this puzzle.

Figure 3a shows the theoretical bands for Si(553)-Au unfolded into the extended Brillouin zone, where they can be easily compared to those obtained from ARPES spectra. Since the theoretical ground state is antiferromagnetic, one need only analyze the bands from a single spin channel. The symbols and curves identify, using the colors from Fig. 1, the atoms that dominate the corresponding wavefunctions. States arising from the magnetic atoms experience an exchange splitting of about 0.5 eV. As a result, for spin-up states the red step-edge band is singly occupied and the blue step-edge band is empty. For spin-down states this situation is reversed, as seen in the density of states, Fig. 3b.

While these magnetic step-edge states are responsible for the 1×6 structural and magnetic periodicity of Si(553)-Au, the remaining features of the band structure have simple 1×1 nonmagnetic character. This is evident from comparing the 1×6 bands to those in Fig. 3d for a simpler 1×1 structure identical to our model but constrained to unit periodicity a_0 and thus having no spin polarization. In this 1×1 structure there is just a single type of step atom and therefore only one corresponding band (green). The remnant of this nonmagnetic band is also visible in the full 1×6 bands, although there its spectral weight at a given momentum is spread out by partial hybridization with its magnetic counterparts.

Both the 1×6 and 1×1 structures give rise to several metallic bands (yellow) with their minima at the zone boundary ZB_{\parallel} . These are the bands detected in ARPES. In the 1×6 case there are a total of four bands in the two spin channels, but the spin-up and spin-down bands are nearly degenerate. In the nonmagnetic 1×1 case there are also four bands but here the degeneracy is broken by the spin-orbit interaction,²² which for simplicity was not included in the 1×6 calculation.²³ The resulting momentum splitting $\delta k_F = 0.04 \text{ \AA}^{-1}$ of the lower band is in excellent agreement with the experimental splitting. The splitting of the upper band is less than half this value and consequently is not resolved in the ARPES data. The predicted Fermi-level crossings of these bands are in qualitative agreement with the measured values: the lower doublet crosses the Fermi level halfway to the

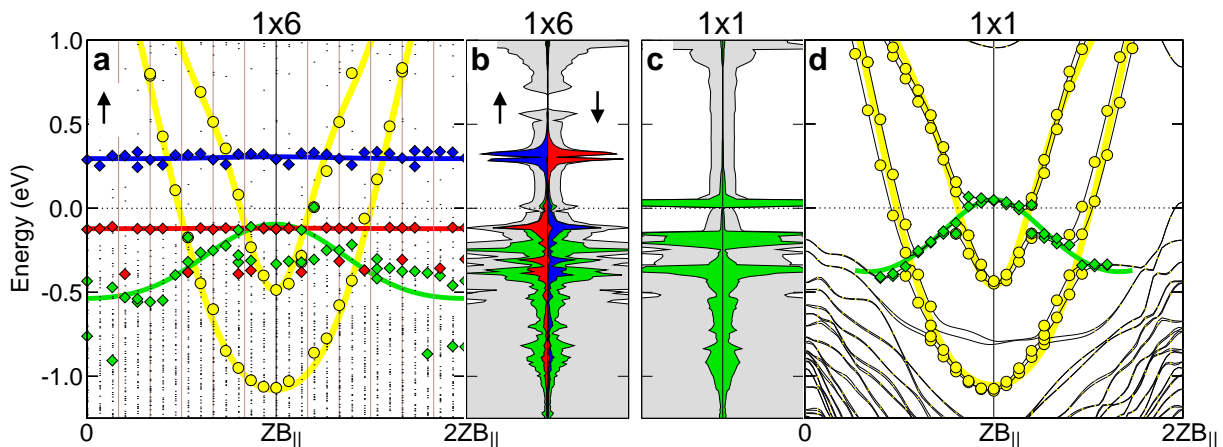


FIG. 3: **Electronic band structure and density of states for Si(553)-Au.** **a–b**, Bands and DOS for the ground-state antiferromagnetic structure of Fig. 1a. The full 1×6 bands are shown unfolded and parallel to the chain direction (ZB_{\parallel} is the boundary of the 1×1 Brillouin zone) along the line halfway to the orthogonal zone boundary ZB_{\perp} . Red and blue diamonds are spin-polarized states from red and blue Si step-edge atoms in Fig. 1a. Only spin-up states are shown here—antiferromagnetic order implies the spin-down states are equivalent but with red and blue reversed, as seen in the DOS. Green diamonds are non-polarized states from green Si step-edge atoms. Yellow circles are bonding (lower) and antibonding (upper) states from the Au chains. Curves show schematic energy bands without hybridization. **c–d**, Bands and DOS for the same model when it is constrained to 1×1 periodicity, for which the ground state is not spin-polarized. Spin-orbit coupling, included in the bands but not in the DOS, splits each of the two Au chain states but not the Si step-edge state.

zone center, and the upper doublet about one-fifth of the way.

One feature of the nonmagnetic 1×1 band structure is *not* observed in the ARPES data: the green step-edge band that just crosses the Fermi level in Fig. 3d. Magnetism provides a simple explanation for the apparent absence of this band. Above a temperature scale set by the energy gained from spin polarization, thermal fluctuations between polarized and unpolarized electron states will broaden the step-edge bands. The magnitude of the broadening is roughly the exchange splitting, 0.5 eV. The resulting reduction in intensity makes the step-edge bands essentially invisible compared to the sharp Au bands, which are not affected by the spin polarization at the step edge. In this sense the experimental absence of a sharp step-edge band constitutes additional evidence for a spin-polarized ground state.

We now briefly summarize our predictions for magnetism in Si(557)-Au, which are qualitatively similar to those for Si(553)-Au, and defer a detailed discussion. Despite having a more complicated arrangement of spins, the surface has a simpler 1×2 periodicity which persists even if spin polarization is suppressed. Magnetism leads to quantitative but not qualitative structural changes: a smaller downward displacement of the magnetic step-edge atoms and a smaller upward displacement of the magnetic restatoms. Therefore we do not predict any higher-order periodicity to mark the onset of magnetism at low temperature.

Earlier theoretical studies of Si(557)-Au included spin-orbit coupling but not spin polarization.⁷ The resulting prediction of momentum-split Au bands were in good agreement with experiment. But these studies also

predicted Si step-edge and restatom bands not seen in ARPES.^{4,10,12} This discrepancy is resolved in the magnetic ground state: the exchange splitting pushes the two occupied spin bands down to 0.4–0.5 eV below the Fermi level, and the two unoccupied spin bands up to 0.1–0.2 eV above the Fermi level. This exchange splitting is similar to the splitting in Si(553)-Au. Thermal fluctuations between polarized and unpolarized states will likewise broaden these step-edge and restatom bands, rendering them invisible to ARPES while leaving the momentum-split Au bands unaffected.

We anticipate that spin-polarized states in silicon are not limited to Si(553)-Au and Si(557)-Au: the key structural element—a graphitic step edge—is known to exist on other stepped silicon surfaces as well.⁴ Direct experimental tests of our predictions using, for example, spin-polarized STM^{24,25} or spin-polarized photoemission²⁶ will be an important next step, and will provide important information about the nature of the magnetic ordering.

To set the stage for such tests it is helpful to estimate the magnitude of the spin interactions within a simple nearest-neighbor Heisenberg Hamiltonian. From DFT total-energy calculations of different spin configurations on Si(553)-Au we find antiferromagnetic coupling ($J_{\parallel} = 15$ meV) along the steps and weaker, ferromagnetic coupling ($J_{\perp} = -0.3$ meV) across the steps. We also find that the magnitude, and even the sign, of these couplings can be changed by doping electron or holes into the Si(553)-Au surface states. It is well-established that surface states on the closely related Si(111)-Au surface can be electron-doped by adsorbates (e.g. silicon adatoms) on the surface, and that the concentration of this ad-

sorbate population can be controlled to some extent.²¹ No such studies have yet been reported for Si(553)-Au or Si(557)-Au, but the possibility of tuning surface magnetism using surface chemistry suggests a wealth of new research possibilities.

Linear chains of spin-polarized atoms provide atomically perfect templates for the ultimate memory and logic, in which a single spin represents a bit. Here the spins are locked into a self-assembled rigid lattice on a substrate that is compatible with silicon technology. One potential application is the spin shift register recently proposed theoretically by Mahan.²⁷ This device requires a one-dimensional chain of identical atoms each with spin $S = 1/2$. When an additional electron is conducted along the chain, each spin state is shifted by one atom—the spin analogue of a standard shift register memory device. The arrangement of spins is arbitrary and there is no requirement of long-range order. However, two other important criteria must be satisfied: in the ground state each atom must have one electron, and the atoms must have correlated electronic states. The first criterion is indeed satisfied by the spin-polarized atoms on Si(553)-Au and Si(557)-Au. In previous work we showed that the electronic states of singly-occupied silicon dangling bonds are indeed strongly correlated.²⁸

Another potential application is the storage of information in single magnetic atoms.²⁹ Toward this end, Hirjibehedin *et al.* recently used spin excitation spectroscopy to demonstrate that the orientation of an individual spin can be measured with an STM.³⁰ For information storage the stability of this orientation, for example from coupling of the spin to the substrate, is critical. This coupling is most likely to be substantial when the substrate is anisotropic at the atomic scale. In the experiments of Hirjibehedin this anisotropy was engineered by creating Cu₂N islands that break the fourfold symmetry of the Cu(001) substrate. In the Si(553)-Au and related vicinal silicon surfaces this anisotropy arises naturally at the step edge. The investigation of spin-lattice coupling in these magnetic silicon surfaces is an important next step toward the ultimate goal of spintronics with single spins.

Methods

First-principles total-energy calculations were used to determine equilibrium geometries and relative energies of the models in Fig. 1 and their variants. The calculations were performed in a slab geometry with six or more layers of Si plus the reconstructed top surface layer and a vacuum region of at least 10 Å. All atomic positions were relaxed, except the bottom Si layer and its passivating hydrogen layer, until the largest force component on every atom was below 0.02 eV/Å. Total energies and forces were calculated within the PBE generalized-gradient approximation³¹ to density-functional theory (DFT) using projector-augmented-wave potentials, as implemented in VASP^{32,33}. The plane-wave cutoff for all calculations was 250 eV.

The sampling of the surface Brillouin zone was chosen according to the size of the surface unit cell and the relevant precision requirements. For the 1×6 reconstruction of Si(553)-Au shown in Fig. 1(a,b), the equilibrium geometries and total energies of nonmagnetic, ferromagnetic, and antiferromagnetic configurations were calculated using 6×6 zone sampling, with convergence checks using 10×10 sampling. For the 1×2 reconstruction of Si(557)-Au shown in Fig. 1c, the equilibrium geometries and total energies of nonmagnetic, ferromagnetic, and antiferromagnetic configurations were calculated using 2×8 zone sampling, with convergence checks using 2×16 sampling.

Exchange coupling constants J_{\parallel} and J_{\perp} for Si(553)-Au were extracted from DFT total energies. Supercells containing two spins on each of two adjacent steps were constructed with the four possible unique spin configurations. The DFT total energies were fit to a nearest-neighbor classical Heisenberg Hamiltonian. The numerical reliability of the coupling constants was analyzed with respect to Brillouin-zone sampling, plane-wave cutoff, and relativistic treatment, and the dependence of the coupling constants upon charge doping of the surface states was investigated (see Supplementary Information).

The simulated STM images in Fig. 2 were calculated using the method of Tersoff and Hamann³⁴. For this filled-state image we integrated the local density of states (LDOS) over a 0.5-eV energy window of occupied states up to the Fermi level. The simulated STM topography under constant-current conditions was obtained by plotting the height at which the integrated LDOS is constant.

* The final version of this draft preprint was published as Nat. Commun. **1:58** (2010) and is available at <http://dx.doi.org/10.1038/ncomms1056>.

¹ Červenka, J., Katsnelson, M. I. & Flipse, C. F. J. Room-temperature ferromagnetism in graphite driven by two-dimensional networks of point defects. *Nature Phys.* **5**, 840–844 (2009).

² Lee, H., Son, Y. W., Park, N., Han, S. W. & Yu, J. J. Mag-

netic ordering at the edges of graphitic fragments: Magnetic tail interactions between the edge-localized states. *Phys. Rev. B* **72**, 174431 (2005).

³ Zabala, N., Puska, M. J. & Nieminen, R. M. Spontaneous magnetization of simple metal nanowires. *Phys. Rev. Lett.* **80**, 3336–3339 (1998).

⁴ Crain, J. N. *et al.* Chains of gold atoms with tailored electronic states. *Phys. Rev. B* **69**, 125401 (2004).

- ⁵ Erwin, S. C. & Weitering, H. H. Theory of the honeycomb chain-channel reconstruction of $M/\text{Si}(111)-(3\times 1)$. *Phys. Rev. Lett.* **81**, 2296–2299 (1998).
- ⁶ Barke, I. *et al.* Low-dimensional electron gas at semiconductor surfaces. *Solid State Comm.* **142**, 617–626 (2007).
- ⁷ Sánchez-Portal, D., Riikonen, S. & Martin, R. M. Role of spin-orbit splitting and dynamical fluctuations in the $\text{Si}(557)\text{-Au}$ surface. *Phys. Rev. Lett.* **93**, 146803 (2004).
- ⁸ Robinson, I. K., Bennett, P. A. & Himpsel, F. J. Structure of quantum wires in $\text{Au}/\text{Si}(557)$. *Phys. Rev. Lett.* **88**, 096104 (2002).
- ⁹ Segovia, P., Purdie, D., Hengsberger, M. & Baer, Y. Observation of spin and charge collective modes in one-dimensional metallic chains. *Nature* **402**, 504–507 (1999).
- ¹⁰ Losio, R. *et al.* Band splitting for $\text{Si}(557)\text{-Au}$: is it spin-charge separation? *Phys. Rev. Lett.* **86**, 4632–4635 (2001).
- ¹¹ Altmann, K. N. *et al.* Electronic structure of atomic chains on vicinal $\text{Si}(111)\text{-Au}$. *Phys. Rev. B* **64**, 035406 (2001).
- ¹² Ahn, J., Yeom, H., Yoon, H. & Lyo, I.-W. Metal-insulator transition in Au atomic chains on Si with two proximal bands. *Phys. Rev. Lett.* **91**, 196403 (2003).
- ¹³ Barke, I., Zheng, F., Rugheimer, T. K. & Himpsel, F. J. Experimental evidence for spin-split bands in a one-dimensional chain structure. *Phys. Rev. Lett.* **97**, 226405 (2006).
- ¹⁴ Riikonen, S. & Sánchez-Portal, D. Ab-initio study of the double-row model of the $\text{Si}(553)\text{-Au}$ reconstruction. *Surf. Sci.* **600**, 1201–1206 (2006).
- ¹⁵ Riikonen, S. & Sánchez-Portal, D. Systematic investigation of the structure of the $\text{Si}(553)\text{-Au}$ surface from first principles. *Phys. Rev. B* **77**, 165418 (2008).
- ¹⁶ Crain, J. N. *et al.* Fractional band filling in an atomic chain structure. *Phys. Rev. Lett.* **90**, 176805 (2003).
- ¹⁷ Crain, J. N. & Pierce, D. T. End states in one-dimensional atom chains. *Science* **307**, 703–706 (2005).
- ¹⁸ Ahn, J. R., Kang, P. G., Ryang, K. D. & Yeom, H. W. Coexistence of two different Peierls distortions within an atomic scale wire: $\text{Si}(553)\text{-Au}$. *Phys. Rev. Lett.* **95**, 196402 (2005).
- ¹⁹ Snijders, P. C., Rogge, S. & Weitering, H. H. Competing periodicities in fractionally filled one-dimensional bands. *Phys. Rev. Lett.* **96**, 076801 (2006).
- ²⁰ Crain, J. N., Stiles, M. D., Stroscio, J. A. & Pierce, D. T. Electronic effects in the length distribution of atom chains. *Phys. Rev. Lett.* **96**, 156801 (2006).
- ²¹ Erwin, S. C., Barke, I. & Himpsel, F. J. Structure and energetics of $\text{Si}(111)-(5\times 2)\text{-Au}$. *Phys. Rev. B* **80**, 155409 (2009).
- ²² Koelling, D. D. & Harmon, B. N. Technique for relativistic spin-polarized calculations. *J. Physics C Solid State Phys.* **10**, 3107–3114 (1977).
- ²³ The spin-orbit interaction strongly affects Au states but has only a small influence on the magnitude of the Si spin-spin interactions (see Supplementary Information, Table III) and was therefore only included in the calculation of Fig. 3d.
- ²⁴ Bode, M. Spin-polarized scanning tunnelling microscopy. *Rep. Prog. Phys.* **66**, 523–582 (2003).
- ²⁵ Wiesendanger, R. Spin mapping at the nanoscale and atomic scale. *Rev. Mod. Phys.* **81**, 1495–1550 (2009).
- ²⁶ Osterwalder, J. Spin-polarized photoemission. *Lect. Notes. Phys.* **697**, 95–120 (2006).
- ²⁷ Mahan, G. D. Spin shift register from a one-dimensional atomic chain. *Phys. Rev. Lett.* **102**, 016801 (2009).
- ²⁸ Hellberg, C. S. & Erwin, S. C. Strongly correlated electrons on a silicon surface: Theory of a Mott insulator. *Phys. Rev. Lett.* **83**, 1003–1006 (1999).
- ²⁹ Otte, A. F. Can data be stored in a single magnetic atom? *Europhysics News* **39**, 31–34 (2008).
- ³⁰ Hirjibehedin, C. F. *et al.* Large magnetic anisotropy of a single atomic spin embedded in a surface molecular network. *Science* **317**, 1199–1203 (2007).
- ³¹ Perdew, J. P., Burke, K. & Ernzerhof, M. Generalized gradient approximation made simple. *Phys. Rev. Lett.* **77**, 3865–3868 (1996).
- ³² Kresse, G. & Hafner, J. Ab initio molecular dynamics for liquid metals. *Phys. Rev. B* **47**, 558–561 (1993).
- ³³ Kresse, G. & Furthmüller, J. Efficient iterative schemes for ab initio total-energy calculations using a plane-wave basis set. *Phys. Rev. B* **54**, 11169–11186 (1996).
- ³⁴ Tersoff, J. & Hamann, D. R. Theory of the scanning tunneling microscope. *Phys. Rev. B* **31**, 805–813 (1985).

Acknowledgements

Helpful conversations with David L. Huber are gratefully acknowledged. This work was supported by the Office of Naval Research, and by the NSF under awards No. DMR-0705145 and DMR-0084402 (SRC). Computations were performed at the DoD Major Shared Resource Center at AFRL.